https://doi.org/10.5194/nhess-2021-47
Preprint. Discussion started: 15 March 2021

Natural Hazards and Earth System Sciences Discussions

Rapid assessment of urban mega-gully and landslide events with Structure-from-Motion techniques validates link to water resources infrastructure failures.

Napoleon Gudino-Elizondo[1,2], Matthew W. Brand[2], Trent W. Biggs[3], Alvaro Gomez-Gutierrez[4], Eddy Langendoen[5], Ronald Bingner[5], Yongping Yuan[6], Brett F. Sanders[2]

[1]Instituto de Investigaciones Oceanológicas, Universidad Autónoma de Baja California, Ensenada, 22760, México.
[2]Department of Civil and Environmental Engineering, University of California, Irvine, 92697, USA.
[3]Department of Geography, San Diego State University, San Diego, 92182-4493, USA
[4]Research Institute for Sustainable Territorial Development, University of Extremadura, Cáceres, Spain
[5]National Sedimentation Laboratory, Agricultural Research Service, USDA, Oxford, 38655, USA
[6]U.S. Environmental Protection Agency, Office of Research and Development, Research Triangle Park, Durham, 27711, USA

Correspondence to: Napoleon Gudino-Elizondo (ngudino@uabc.edu.mx)

Abstract. Mega-gullies and landslides pose significant hazards to urban development on steep terrain. Water resources infrastructure failures (WRIFs), such as leaks and breaks in water supply pipes, have been postulated as a trigger of mass movement events but data for validation has been challenging to acquire since earthwork proceeds quickly after events to repair roads and other infrastructure. Urban development in Tijuana, Mexico was monitored for a five-year period to document the occurrence of mega-gullies and landslides, including sediment volumes. A rapid assessment approach was developed based on photogrammetric observations from an unmanned aerial vehicle (UAV) and Structure from Motion (SfM) digital processing. Three hazardous mass-movement events were observed including two mega-gullies and one landslide. Furthermore, all three events were linked to WRIFs. Frequency analysis points to the annual probability of a WRIF-based erosion event in the range of 40-60%, which is far higher than design levels typically used for urban stormwater infrastructure (5-10%). Additionally, sediment modelling points to WRIF-based erosion as a non-negligible contributor to sediment generation. These results suggest that WRIFs are a significant contributor to erosion hazards facing urban development on steep terrain, and call for expanded monitoring to characterize the occurrence and modes of WRIF-based erosion events.

1 Introduction

Mega-gullies and landslides pose significant hazards to urban development on steep terrain (Sidle et al., 2011; Anderson et al., 2014; Imwangana et al., 2014; Fu et al., 2020). Mega-gullies are erosional features with widths and depths of several meters, while landslides are downslope mass wasting under the influence of gravity. Both mass movement mechanisms can undermine or damage housing and civil infrastructure, while landslides present life-threatening safety risks (Calvello et al., 2016; Peng et

https://doi.org/10.5194/nhess-2021-47
Preprint. Discussion started: 15 March 2021


Natural Hazards and Earth System Sciences Discussions

al., 2017; McAdoo et al., 2018). Mega-gully and landslide hazards are increasing at a time of rapid urbanization as a result of limited oversight of planning and construction as well as socio-economic pressures that force populations to settle in high-hazard areas (Hardoy et al., 2013; Retief et al., 2016; Miller et al., 2019). Moreover, mass movement hazards are concentrated in developing middle- and low-income regions of the world where unregulated settlement occurs on steep slopes (Anderson et al., 2014). For example, in Latin America, expanding poor areas on the periphery often have steep slopes (Sepúlveda and Petley, 2015) and/or poor infrastructure that is vulnerable to erosion and destabilization (Griffin and Ford 1980; Davis, 2006; Biggs et al., 2010, 2014).

Successful hazard mitigation requires understanding of mechanisms and triggers. In the case of urban mega-gullies, the dominant mechanisms identified in the literature relate to surface runoff generated by rainfall during storm events, exacerbated by flow path concentration on road networks (Imwangana, et al., 2014). The role of rain-generated runoff in gully formation has been highlighted in studies of both agricultural and urban areas (Valentin, et al., 2005). Landslide hazard, similarly, is thought to be controlled by a combination of inherent slope instability exacerbated by hydraulic erosion (Xu et al., 2015) and high soil moisture content following storms (Kuo et al., 2018; Valenzuela et al., 2018; Zhuo et al., 2019; Marino et al., 2020). However, there is increasing evidence that Water Resources Infrastructure Failures (WRIFs) are an important trigger of mass movement hazards within urban development on steep slopes. WRIFs include cracks, leaks, and breaks of water supply, drainage and/or sewerage pipes that are buried beneath the ground surface. WRIFs have been linked to the generation of sinkholes (Kim et al., 2018), amplified erosion (Guo et al., 2013), and destabilization of soil (Van Zyl, et al., 2013). Nevertheless, little is known about the frequency and severity of mass movement hazards linked to WRIFs, which cannot be predicted or modelled from geomorphic and hydrologic processes occurring at smaller spatial scales but is necessary to quantify in order to develop a complete description of the socio-geomorphology (Ashmore, 2015) of rapidly urbanizing regions. Monitoring of mega-gullies and landslides in urban areas is challenging, as earthwork typically proceeds quickly after an event to clean up or restore sites impacted by displaced sediment, and access for monitoring faces safety concerns related to slope instabilities.

Structure-from-motion (SfM) photogrammetry can safely monitor mass movement features with either on-ground or airborne platforms (Nadal-Romero et al., 2015; Eltner et al., 2016; Kaiser et al., 2018; Fugazza et al., 2018; James et al., 2019; Ma et al., 2020), and can be deployed quickly after an event to scan a site—providing data that can be subsequently processed to estimate volumes of sediment displaced and the dimensions of erosional features. This paper reports the results of a five-year observational study whereby SfM was deployed in a rapid-response mode to document the frequency and magnitude of mass movement hazards associated with WRIFs, and to quantify the amount of sediment generation compared to other processes. To our knowledge, no study has examined the impact of WRIF on hazardous mass movement events and its impacts on sediment budget at the watershed scale (Ionita et al., 2015; Poesen, 2018). The study is conducted in Los Laureles Canyon watershed (LLCW), a rapidly urbanizing area of Tijuana, Mexico. Here, construction of housing and roadways on steep slopes created conditions conducive to increase soil erosion, sediment generation, slope instabilities and flood hazards (Biggs et al., 2010, Luke et al., 2018, Goodrich et al., 2020). Moreover, local authorities (Chief of Civil Protection, Tijuana Mexico, personal

https://doi.org/10.5194/nhess-2021-47
Preprint. Discussion started: 15 March 2021


Natural Hazards and Earth System Sciences Discussions

communication, 2016) have observed that WRIFs trigger mega-gullies and landslides that pose life-threatening hazards. The objectives of this paper are three-fold: (1) to report the effectiveness of SfM photogrammetric techniques for rapid erosion assessment following WRIF events, (2) to document the frequency and magnitude of sediment mobilization from WRIF events, and (3) to evaluate the significance of WRIF events with respect to mass movement hazards and sediment budgets at neighborhood- and watershed-scales.

The remainder of the paper is organized as follows: Section 2 (Methods) presents a site description, SfM-based observational methods, and watershed modeling methods to sediment budgets; Section 3 (Results) presents data on the frequency and magnitude of WRIF-based mass movement and neighborhood- and a comparison of WRIF-based fluxes to other mechanisms of sediment generation. The paper concludes with discussion (Section 4) and conclusions (Section 5).

2 Materials and Methods

2.1 Site Description

The Los Laureles Canyon Watershed (LLCW) is an urbanizing binational catchment that overlaps the western-most portion of the USA – Mexico border. LLCW flows from the city of Tijuana, Mexico, into the Tijuana River Estuarine Reserve, USA (Fig. 1). Sediment from excess erosion and solid waste transported in the channel network from Tijuana have impaired the estuarine ecosystem (Weis et al., 2001).

https://doi.org/10.5194/nhess-2021-47
Preprint. Discussion started: 15 March 2021

Natural Hazards and Earth System Sciences
Discussions

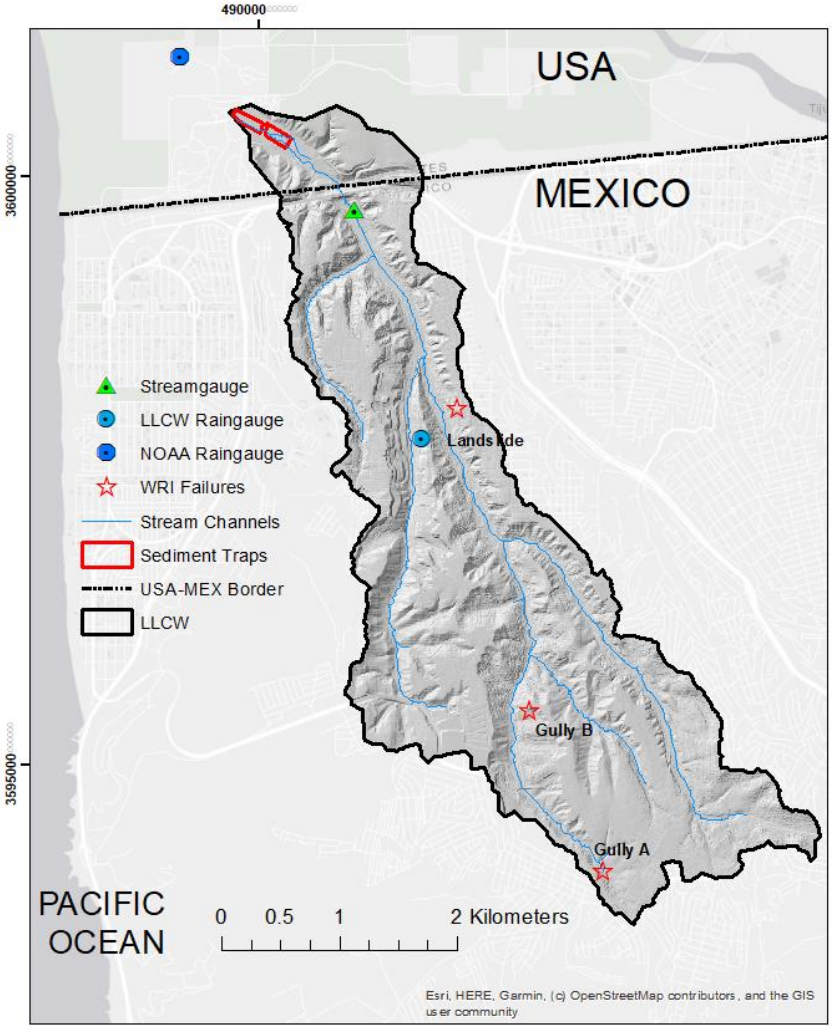

Figure 1. Los Laureles Canyon Watershed (LLCW), locations of water resources infrastructure failures (WRIFs), and field equipment. Base map from © OpenStreetMap contributors, 2020. Distributed under a Creative Commons BY-SA License.

85

The climate in LLCW is Mediterranean, with a wet winter, dry summer and an average annual precipitation of 240 mm. The regional geology includes marine and fluvial deposits of conglomerate, sandy conglomerate, and siltstone of the San Diego formation (Gastil et al., 1975, Minch et al., 1984). Soils are generally sandy with a wide range of cobble fraction, and are dominated by steep slopes (15 degrees, average). Urbanization in LLCW started in 1962, with most urbanization occurring
90 between 1980 and 2002 (Biggs et al., 2017) in the form of unauthorized housing developments ("invasiones"). Construction of poorly planned housing and roadways on steep slopes created conditions conducive to concentrate storm-water runoff and increase soil and gully erosion, slope instabilities, and failures in WRI. The socioeconomic status of residents in the LLCW is

https://doi.org/10.5194/nhess-2021-47
Preprint. Discussion started: 15 March 2021


Natural Hazards and Earth System Sciences Discussions

low in the southern part of the watershed and in the areas with infrastructure failure as evidenced by a high marginality index and a low fraction of homes with piped water or drainage as compared with other areas of Tijuana (Biggs et al., 2014).

2.2 Study Design

Hydrologic conditions, slope instabilities, and sediment generation rates were monitored in the LLCW for a 5-year period beginning in January 2013 and ending in April 2018. To measure rainfall, a tipping-bucket rain gauge station ("LLCW raingage" in Fig. 1) was installed in the watershed, and to measure stream stage, a pressure transducer (PT) (Solinst, water level logger) was installed in a concrete channel at the watershed outlet and logged conditions at 5-minute intervals (Fig. 1). Upon detection of flow at the watershed outlet, field personnel travelled to the site, performed a visual inspection of site conditions, and, upon observation of mega-gullies and landslides, collected two types of data about the WRIF erosional features: (1) photogrammetric surveys (RGB images) were performed with a nonmetric camera (GoPro Hero3+) from either a ground-based or aerial platform, and (2) ground control points (GCPs) were acquired by differential GPS (Magellan Pro Mart 3) with sub-centimeter to 5 cm accuracy (Magellan Systems Corporation, San Dimas, USA). These primary data were used to create Digital Surface Models (DSMs), and in turn, estimates of sediment volumes and their impacts on sediment budget, as well as to document safety hazards to the people living in the watershed and downstream ecosystems.

A long-term record of rainfall is available from the NOAA Tijuana River Estuary gauging station, located near the outlet of the LLCW, which provides daily rainfall for the period 1980 to 2018. These data are used here to estimate the return period of storm events during the study period. Data from the tipping-bucket rain gauge (LLCW Raingage in Fig. 1) were used to force a watershed erosion model, validated with stream gauge data and observed sediment loads at the outlet. The model was used to compare sediment generation from WRIF features with the other watershed processes described in section 2.4.

2.3 Image acquisition and processing

Photogrammetric surveys using a nonmetric camera (GoPro Hero3+) were completed using either an Unmanned Aerial System (UAS) (DJI, Phantom2) or a telescoping painter's pole (approximately 2-3 m long). The UAS is advantageous for relatively large and wide erosional features compared with the painter's pole, which can better access relatively small, narrow, and deep erosional features (Gudino-Elizondo et al., 2018a, Taniguchi et al., 2018). Images were acquired once per second using the time-lapse capture mode from different angles to ensure a high overlap between photographs and to reduce the shade in each image (Castillo et al., 2015) and doming deformations (James and Robson, 2014).

The sediment volume mobilized was estimated using a four-step procedure: (1) Imagery were combined with a subset of the GCPs to calibrate the camera and produce Structure from Motion (SfM) point clouds following general workflows (Agisoft LCC, Russia, Version 1.4.4), (2) SfM point clouds were converted to a digital surface model (DSM) (Agisoft LCC, Russia, Version 1.4.4), (3) erosional volumes were computed (ArcGIS 10.6.1, ESRI, Redlands, California) by subtracting the DSM from a reference DSM representative of the pre-event land surface (Wheaton et al., 2010), and (4) the difference DSM was

https://doi.org/10.5194/nhess-2021-47
Preprint. Discussion started: 15 March 2021


Natural Hazards and Earth System Sciences Discussions

integrated to calculate the total sediment volume. Volumes were converted to mass using a bulk density of 1,600 kg /m^3 corresponding to very fine sand (USDA, 2018).

Pre-event topography was based on either a 2014 aerial LIDAR survey (1 m resolution DSM with a 0.11 m vertical RMSE, NOAA, 2014), or with UAS-based DSMs generated with imagery collected before the failure event (Table 1). The horizontal and vertical RMSE of the DSM, or geo-registration error, was estimated using the subset of the GCPs not used to produce the SfM point cloud, called Error Control Points (ECPs). Previous work indicates that 4 to 5 GCPs with a few additional ECPs are adequate for SfM processing (James et al., 2017). The RMSE for the DSM creation was computed as the square root of the sum of the squared errors for each ECP (Alfonso-Torreño et al., 2019).

Table 1. Structure from Motion survey description and data acquisition

Erosional feature	**Landslide**	**Mega-gully A**	**Mega-gully B**
Acquisition platform	UAV	UAV	Pole
Date of survey	05/22/2015	09/23/2015	02/17/2017
Number of pictures	62	115	899
Altitude (m)	75 m	30 m	4 m
Area covered (m^2)	38,400	1,800	2,800
Ground sample distance (cm/pxl)	10	4	3
Point density (points/m^2)	11	48	261
Numbers of GCPs	8	8	12
Numbers of ECPs	6	6	10
RMSE of ECPs (horizontal, vertical) (cm)	(3, 7)	(3, 5)	(3.5, 5)
Pre-event topography	LIDAR	SfM	SfM

As another check on accuracy, the dimensions of invariant features (concrete pads, water pipes, etc.) were directly measured in the field and compared to length estimates from the SfM point cloud as described in Gudino-Elizondo et al. (2018a). Additionally, pre- and post-event ground elevations were compared along transects outside the disturbed region where no topographic change was observed.

2.4 Watershed Modeling

The Annualized AGricultural Non-Point Source (AnnAGNPS) model (Bingner et al., 2015) was applied to the LLCW to simulate discharge and sediment load during storm events and to develop an inventory of sediment generation rates by mechanism at the watershed scale. The AnnAGNPS model was previously calibrated and validated for runoff and observations of sediment generation in LLCW (Gudino-Elizondo et al., 2018a, 2018b, 2019b), and the applications here rely on this

https://doi.org/10.5194/nhess-2021-47
Preprint. Discussion started: 15 March 2021


Natural Hazards and Earth System Sciences Discussions

calibration. The simulation period was 2012 to 2017 water years to match the observational period. Sediment excavation rates from the sediment traps at the LLCW outlet (Fig. 1) were used for model calibration. The sediment traps were excavated annually from 2007–2012 (N = 7). Uncertainties in the modeled sediment yield were previously reported by Gudino-Elizondo et al. (2019b) as approximately 10%, with a normalized RMSE of 48%.

Measurements and modeling supported an inventory of sediment generation and load from four mechanisms: (1) sheet and rill erosion, (2) gully erosion, (3) channel erosion, and (4) erosion from WRIF. Sediment generation was considered as the total mass of sediment mobilized, while the sediment load was the quantity of sediment observed at the watershed outlet. Sediment load from WRIF was calculated by multiplying the erosion volume per event times the Sediment Delivery Ratio (SDR). For mega-gullies, the SDR was set to 1 based on field observations and modeling work described in Gudino-Elizondo et al. (2019b). Conversely, the SDR was set to zero for the landslide based on field observations that displaced sediment was intercepted by the road network and mechanically removed or repositioned on the hillslope (Vigiak et al., 2012). Of course, subsequent rainfall events may cause the repositioned sediment to be later mobilized and moved towards the stream network, so our estimates of load correspond only to the period of observation.

2.5 Hazard assessment from water resources infrastructure failure

Reports of the damage caused from mega-gullies and landslide were compiled from residents and local agencies. Primary data from the three events are described, including impacts to transportation, housing, urban infrastructure and downstream ecosystems and communities in the study watershed. The specific soil loss (SSL) of the WRIF mega-gullies was calculated as the total erosion (m^3) normalized by the watershed area (m^2) and was then compared to the observed SSL in the study watershed and to other studies reported in the literature. A detailed description of safety hazards and the contribution to the total sediment budget of each WRIF event is described in section 3.

3 Results

A total of 14 storm events were observed during the 5-year study period, based on a flow threshold of 1 $m^3 s^{-1}$ (or ~15 cm of water in the channel) at the gaging station, which corresponds to a depth of rainfall ranging from 6.5 to 13 mm. The total depth of the 14 storms was 322 mm, or 35% of the total rainfall (907 mm, 181 mm y^{-1}) for the 5-year period. Mass movement from WRIFs were observed during three of these events, each characterized by a 1-2-year return period. WRIFs leading to mass movement were not observed between storm events or during smaller storm events (< 23 mm).

3.1 SfM surveys and social impacts by event

Three storm events caused WRIFs that led to hazardous mass movements. One event involved a landslide and two involved formation of mega-gullies. The detailed observations of each feature are described in sections 3.1.1 to 3.1.3.

https://doi.org/10.5194/nhess-2021-47
Preprint. Discussion started: 15 March 2021

Natural Hazards and Earth System Sciences
Discussions

3.1.1 Landslide

A large landslide occurred during a storm event on 15 May 2015 (Fig. 2). More than 20 houses were damaged affecting more than 100 people (Fig. 2b, 2c). Based on the daily rainfall total (23 mm) and the long-term rainfall record at the NOAA Tijuana River Estuary Gage, the return period of the storm is 1 year. The landslide was attributed to a WRIF based on resident reports that seepage from the slope along with incipient cracks were observed for several days immediately before the failure incident. This observation led to the evacuation of the residents when the evolution of the cracks was evident. The infrastructure failure wetted the soil, and the landslide was then triggered by the rain event. Broken water mains were also observed after the landslide (Fig. 2c, red circle). The dimensions of the landslide are approximately 20 m high and approximately 75 m long, with a maximum width of 40 m measured from the main scarp to the toe of the hill. SfM photogrammetry leads to an estimate for the sediment volume and mass: 19,900 ± 580 m^3 and 31,900 ± 928 metric tons. The reported uncertainties (± value) are obtained by propagating horizontal and vertical RMSEs of the DSMs.

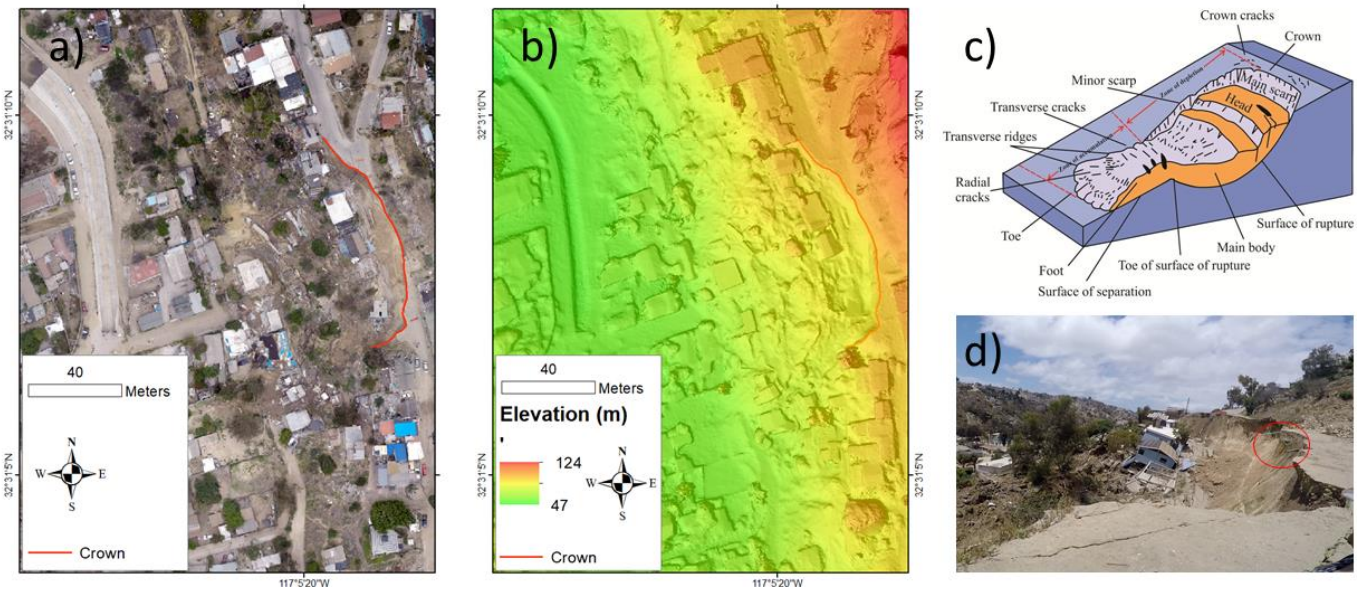

Figure 2. Landslide event on 15 May 2015 triggered by water main leak and rainfall: (a) Orthophoto acquired after the WRIF showing the upper limit of the main scarp (crown) with the red line, and (b) the resulting DEM, (c) a schematic diagram of the anatomy of a landslide (USGS, 2021), and (d) ground-based photographs of the landslide showing broken water mains inside the red circle aligned with the main scarp.

The RMSE (ECPs, n=6) of the DSM obtained from SfM was 3 cm in the horizontal and 7 cm in the vertical coordinates. James and Robson (2012) introduced the relative precision ratio for UAS-SfM applications (i.e., ratio of measurement precision to observation distance), and found that 1:950 indicates acceptable accuracy over a range of scales. For a flight height of 75 m, the James and Robson (2012) standard gives a desired DSM error of 7.8 cm, which compares well with the horizontal and

https://doi.org/10.5194/nhess-2021-47
Preprint. Discussion started: 15 March 2021

Natural Hazards and Earth System Sciences
Discussions

vertical errors estimated here. Elevation differences outside of the disturbed area were 0-7 cm. The mean difference between measured and modeled lengths of objects at the site (e.g., sewer manhole covers) was less than 3 cm. These different methods all suggest the error was less than 7 cm and within the range expected for the observation distance.

3.1.2 Mega-gully A

A mega-gully formed along an unpaved road following a storm event on 15 September 2015. Based on the daily rainfall total (31 mm) and the long-term rainfall record at the NOAA rain gauge, the return period of the storm was 1-2 years. This mega-gully was attributed to a WRIF based on resident reports that leakage from a broken pipe was observed upstream immediately after the failure event (personal communication, Tijuana Metropolitan Planning Institute). In this case, erosion caused by the storm event undermined the water main, which subsequently broke and enlarged the gully as a result of high velocity water jets from the pressurized water main. The mega-gully was 98 m long, with a maximum width of 8 m and maximum depth of 4 m (Fig. 3). The generated sediment mass was estimated as 1,360 ± 65 tons.

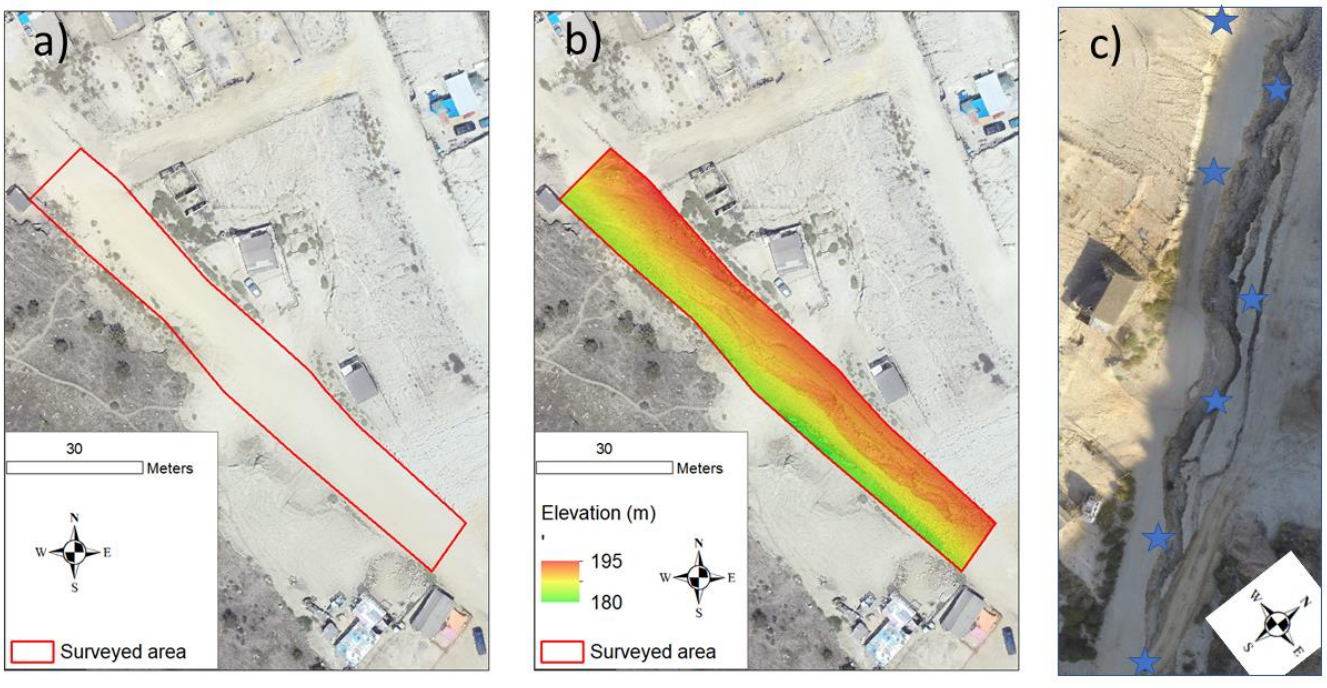

Figure 3. Mega-gully formed on 15 September 15, 2015 by WRIF: (a) Orthophoto acquired before the WRIF showing the extent of the surveyed area centred in the red rectangle, (b) the resulting DEM and (c) an orthophoto acquired after the WRIF, the blue stars represents ground control points.

The RMSE (ECPs, n=6) of the DSM obtained from SfM was 3 cm horizontal and 5 cm vertical. Elevation differences outside of the disturbed area were 0-5 cm. Field measurements of the mega-gully width and depth differed from the SfM-derived width

https://doi.org/10.5194/nhess-2021-47
Preprint. Discussion started: 15 March 2021

Natural Hazards and Earth System Sciences
Discussions

and depth by less than 2 cm on average. This WRIF caused the interruption of water supply for 1 month, affecting more than 300 residents (personal communication, Tijuana Metropolitan Planning Institute). The corresponding erosional feature impacted public transportation and life quality to the neighbourhood for 6-9 months (available Google Earth imagery 11 December2015- 08 August 2016) before the road was repaired.

3.1.3 Mega-gully B

A second mega-gully formed along an unpaved road following a storm event on 16 December 2016. Based on the daily rainfall total (33 mm) and the long-term rainfall record at the NOAA rain gauge, the return period of the storm is 1-2 years. The mega-gully was largest at the upslope position and decreased in cross sectional area with distance from the broken pipeline. The mega-gully was 202 m long, with a maximum width of 10 m and maximum depth of 7 m. Imagery was collected for the SfM processing using a telescoping painter's pole (Fig. 4d), and sediment generation was estimated to be 4,340 ± 408 tons.

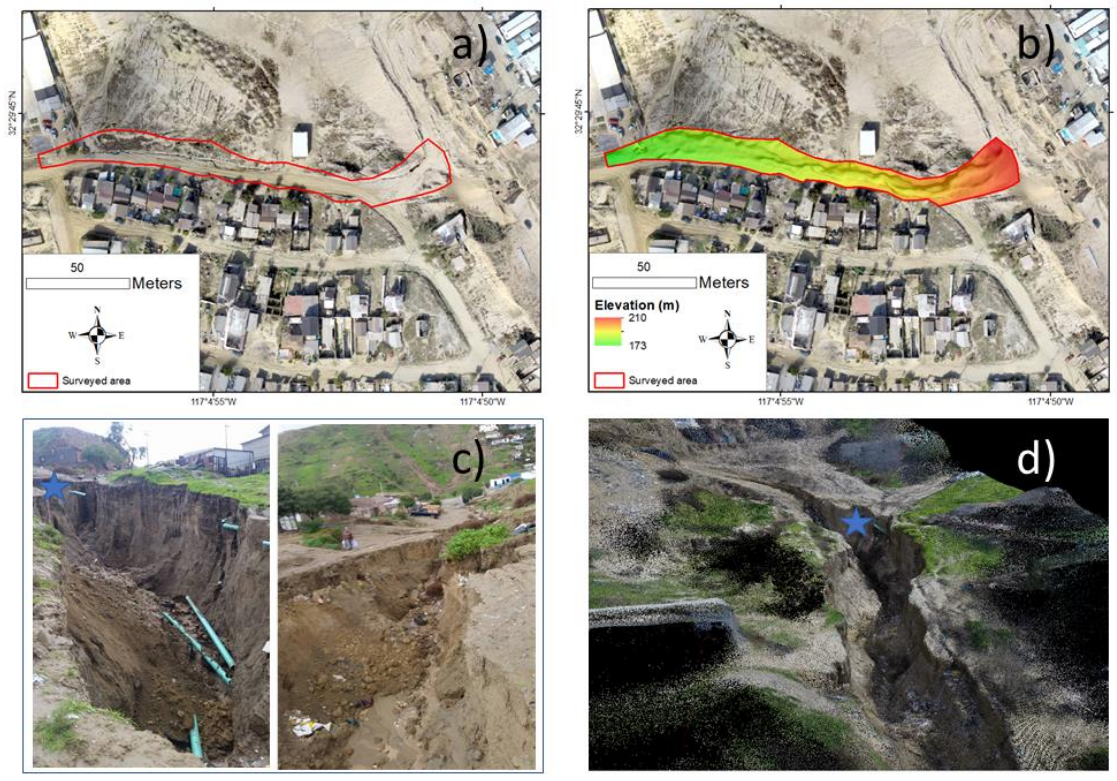

Figure 4. Mega-gully formed on 16 December 2016 triggered by WRIF: (a) Orthophoto acquired before the WRIF showing the extent of the surveyed area centred in the red polygon, (b) the resulting DEM after the WRIF, (c) Images depicting the mega-gully with view angles looking upslope and downslope of the WRIF, and (d) a screenshot of the resulting point cloud.

https://doi.org/10.5194/nhess-2021-47
Preprint. Discussion started: 15 March 2021


Natural Hazards and Earth System Sciences Discussions

The RMSE (ECPs, n=10) of the DSM obtained from SfM was 3.5 cm in the horizontal and 5 cm in the vertical. Elevation differences outside of the disturbed area were 0-5 cm, which is consistent with the accuracy of the method. For example, differences between measured and modelled lengths of not-deforming objects at the site (e.g., water supply pipes shown as blue stars in Fig. 4c and Fig. 4d) were less than 1 cm.

For this second mega-gully event, mass movement was again triggered by erosion that undermined the water main, which subsequently broke and enlarged the gully by discharging piped water directly onto the hillslope. Broken water main pipes were noted during the rapid-response survey (Fig. 4a and 4c). The mega-gully also impacted public transportation and life quality in the neighbourhood for 6 months (based on Google Earth imagery) and interrupted water supply for 1 month, affecting more than 200 people (personal communication, Tijuana Metropolitan Planning Institute).

3.2 Comparison of Sediment Generation Sources

Application of the calibrated AnnAGNPS watershed model to storm events for 2012-2017 yielded daily estimates of rainfall-based sediment generation by sheet and rill erosion, gully erosion and channel erosion. Table 2 presents sediment generation (by mass) on a storm event basis, showing the amount of sediment generation associated with WRIFs measured using SfM, and the simulated total watershed sheet and rill erosion, gully erosion, and channel erosion at the event-scale. Additionally, Fig. 5 shows the relative contribution of WRIF and rainfall-based sediment generation mechanisms.

Table 2. Sediment generation by process during storm events with WRIFs in the Los Laureles Canyon Watershed.

Generation Mechanism (tons)	Landslide event (May 15, 2015)	Mega-gully A event (September 15, 2015)	Mega-gully B event (December 15, 2016)
*Water Resources Infrastructure Failures	31,900	1,360	4,340
**Sheet and Rill	5,310	4,710	12,100
** Rainfall-runoff gullies	10,500	49	160
*Channel Erosion	7,610	2,290	5,910
Total Generation	55,300	8,410	22,500

***Sediment quantified using field measurements, **Sediment quantified using the AGNPS model.**

This analysis shows that mass movement associated with WRIFs was significant on an event basis. Mega-gully B generated 4,340 tons (Table 2), which is approximately 80 times the area-normalized annual erosion rate for gullies (tons/ha) and 10 times the total sediment generated by other rainfall-generated gullies (Gudino Elizondo et al., 2018a, Gudino Elizondo et al., 2018b). The WRIF-triggered landslide mobilized more sediment than all of the rainfall-based processes combined, while the mega-gullies triggered by pipe failures and hydraulic mining were responsible for 16 and 20% of the total sediment generation across the watershed (Fig. 5).

https://doi.org/10.5194/nhess-2021-47
Preprint. Discussion started: 15 March 2021

Natural Hazards and Earth System Sciences
Discussions

The proportion of sediment generated by each erosional process differed markedly between the landslide event and the two mega-gully events (Fig. 5); rainfall-generated gullies contributed more sediment during the landslide event because peak discharge, the main control on gully formation, was higher during the landslide storm event (19.5 cms at the outlet) than during the two mega-gully events (~5 cms) (Gudino-Elizondo et al., 2019b).

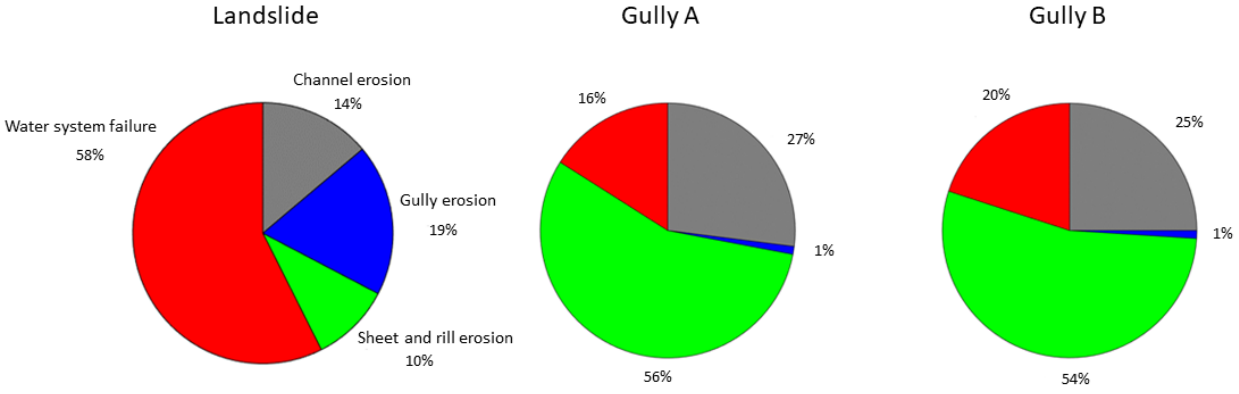

Figure 5. Relative contribution of sheet and rill erosion, gully erosion, channel erosion and water system failure towards sediment generation for three storm events with water resources infrastructure failures.

The total sediment generation and load were computed for the 5-year study period by integrating over all storm events (Table 3). On a five-year basis, WRIFs contributed 5% of the total sediment generation and approximately 2% of the total sediment load at the watershed scale. While the sample size here is small, the frequency of WRIF-based erosional events can be estimated in several ways: three hazard events occurred over a period that had 14 rainfall events (21% of rainfall events), two out of five years had at least one hazard event (40% chance per year), or three events occurred in five years (60% chance per year). The small sample size implies a high degree of uncertainty in all of these estimates; nevertheless, these rates of occurrence are far higher than typical design standards for water resources infrastructure in urban areas. For example, large flood control channels are typically designed with a 0.2-2% annual exceedance probability, and smaller drainage systems in urban areas are often designed for 5-10% annual exceedance probability. Hence, WRIF-based hazards observed during this study are many times more frequent (21-60%) than typical design standards for flood control systems in urban areas (0.2-10%) and thus deserving of greater attention for public safety, infrastructure resilience and environmental protection.

https://doi.org/10.5194/nhess-2021-47
Preprint. Discussion started: 15 March 2021


Natural Hazards and Earth System Sciences Discussions

Table 3. Five-year total sediment generation and load rates (by process), fraction of total generation, and fraction of total load for the Los Laureles watershed.

Generation Mechanism (tons)	5-years Total Sediment Generation	5-years Total Sediment Load	Fraction of Total Generation (%)	Fraction of Total Load (%)
WRIF	37,566	5,696	5	2
Sheet and Rill	258,592	197,538	34	48
Rainfall-runoff gullies	228,207	75,253	30	18
Channel Erosion	234,150	131,212	31	32
Total	758,515	409,699	100	100

3.3 Comparison to Previous Observations

The mega-gullies observed here are large compared to rainfall-generated gullies surveyed in the study area (Gudino-Elizondo et al., 2018a), which had a mean gully width of 1.5 m and a mean depth of 0.5 m. In contrast, mega-gully A is up to 8 m wide and 4 m deep, and mega-gully B is up to 10 m wide and 7 m deep. Mega-gullies A and B are also long with lengths of 100 and 200 m, respectively. Mega-gullies A and B were also more developed than rainfall-generated gullies, with greater connectivity to the stream channel, which enhances sediment delivery to the stream network.

Figure 6 shows that the specific soil loss (SSL, the average depth of soil loss in the watershed) from mega-gully B was exceptionally high compared to rainfall-runoff gullies in the LLCW (Gudino-Elizondo et al., 2018a) and compared to sites reported by Castillo and Gómez (2016), which included sites spanning different land uses and precipitation regimes. The SSL from mega-gully A was comparable to other gullies observed in the study watershed, which has higher rates of SSL than the set of sites reported by Castillo and Gómez (2016).

https://doi.org/10.5194/nhess-2021-47
Preprint. Discussion started: 15 March 2021

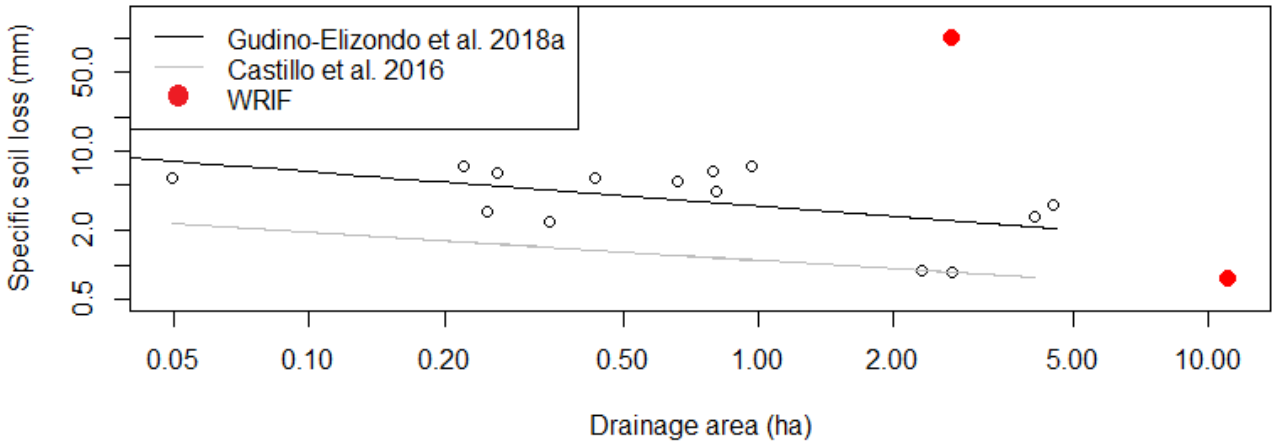

Figure 6. Specific soil loss of mega-gullies caused by WRIF (red dots) compared to previously reported gullies in Tijuana, Mexico (circle points and black line, Gudino-Elizondo et al., 2018a) and trends for ephemeral gullies reported from other sites (gray line, Castillo and Gómez 2016).

The landslide caused by the WRIF was the single largest erosional feature observed in the watershed during the study period. Landslides occur throughout Tijuana, with more than 40 landslides from 1992-2012, including a landslide that damaged 19 buildings (Oliva-González et al., 2014), which is comparable to the LLCW slide (20 buildings damaged). However, data describing the sediment displaced by these 40 landslides and potential connections to WRIFs were not available.

4 Discussion

4.1 Rapid methods for monitoring erosional features

Landslides and mega-gullies have complex topographies and are poorly suited to the application of traditional surveying techniques such as total stations, but are well suited to photogrammetric characterization using SfM. In our study, photogrammetric data were effectively captured for mega-gullies roughly 5-10 m wide, 5-10 m deep, and >100 m long using a camera mounted on a telescoping painter's pole, and landslides were safely characterized using a UAS-based platform. The presence of urban infrastructure in photographs (e.g., concrete pads, sewer structures) also presented opportunities for ground control points and accuracy checks. Accuracies achieved from these observations (i.e., 3 cm horizontal RMSE and 5 cm vertical RMSE) are in line with the needs for sediment budget applications (Dietrich, 2016; Alfonso-Torreño et al., 2019). The SfM photogrammetric approach is in many ways ideal for surveying WRIFs because: (1) the camera is lightweight and easily mounted on either a ground-based or aerial platform; (2) SfM requires less field personnel reducing significantly human-based errors and is more time efficient than traditional topographic surveying methods (Carrera-Hernandez et al., 2020); and (3) hardware costs are relatively low. Laser scanning or LIDAR systems could be advantageous compared to photogrammetry in

https://doi.org/10.5194/nhess-2021-47
Preprint. Discussion started: 15 March 2021


Natural Hazards and Earth System Sciences Discussions

terms of point density and data accuracy, but they are typically quite heavy compared to cameras, require more sophisticated spatial referencing systems (e.g., inertial navigation units), often present occlusion artifacts, and are expensive (Izumida et al., 2017; Mazzoleni et al., 2020). Our study demonstrates that both ground-based and UAS-based photogrammetry allow for rapid documentation of hazardous erosional features with minimal equipment and low labor requirements.

4.2. WRIFs and the sediment budget

Stochasticity in WRIFs and WRIF-based sediment hazards is high. Failures may or may not happen in any given storm (here we observed 3 failures in 14 storm events), and when failures occur, the volume of sediment generated across three events varied by over an order of magnitude. This makes it difficult to generalize and estimate sediment generation by infrastructure failure for other events lacking field observations. However, the data do allow a first-order estimate of annual-average sediment generation from WRIFs which is useful for sizing sediment basins that protect downstream ecosystems from excess sedimentation and for estimating average-annual excavation costs. Such estimates would not likely be applicable outside of the LLCW, but the photogrammetric methods deployed here to monitor sediment generation are easily transferrable to other systems, and data on sediment generation from multiple sites would provide a basis for improved understanding and possibly transferrable models.

4.3 Feedbacks between erosion and slope instabilities from WRIFs: opportunities for hazard mitigation

Erosion and hazards produced by WRIFs were either exacerbated or triggered by erosion during storm events. The observed landslide was triggered by a storm event, but the event was preceded by the water main leak. The observed mega-gullies formed after local runoff initially undermined water mains, which then broke and discharged water onto the hillside, triggering more severe gully erosion. This suggests that WRIFs, storm events, and slope instabilities are interdependent. Moreover, this opens the possibility of reducing mass movement hazards through improved design, management and oversight of water resources infrastructure. Whereas rapid urbanization is broadly linked to minimal levels of governance and institutional oversight of urban infrastructure, especially in least-developed countries (Borelli et al., 2018), water resources infrastructure benefit from relatively high levels of planning, design, engineering and oversight (Whittington et al., 2009; Cook, 2011). For example, mass movement hazards could be reduced by aligning water mains away from topographic low spots susceptible to gully formation, and away from hillslopes that may be susceptible to creeping displacements that stress pipes and cause leaks. Pipeline specifications could also be changed to promote greater ductility, or resistance to failure, under hillslope displacement (Honegger et al., 2010; Han et al., 2012). In turn, the water resources infrastructure would benefit from fewer leaks and breaks and higher levels of reliability.

4.4 Implications for hazard mitigation in other urban contexts

Landslides and mega-gullies like those observed in Tijuana have been reported across cities in middle and low-income countries where unregulated settlement occurs on steep hillslopes (Anderson et al., 2014), but also in developed countries. For

https://doi.org/10.5194/nhess-2021-47
Preprint. Discussion started: 15 March 2021

example, in the city of San Diego, California (USA), soil erosion caused by a storm on January 5, 2016 undermined a 30-foot section of sewer causing failure and prompting a spill of more than 6.7 million gallons of untreated sewage that severely eroded the riverbank and negatively impacted downstream ecosystems (Garrick, 2020). Nevertheless, what is clear is that even though the sample size of events reported in this analysis is small, the severity of the events involving WRIFs is high. Housing, transportation, and utilities that serve hundreds of people living in the watershed are impacted by WRIFs in Tijuana. WRIF-based mass movements also contributed a significant amount of sediment to the total watershed load, which negatively impacted habitat and aquatic ecosystems, and further increased downstream infrastructure maintenance costs (Brand et al., 2020). Acknowledging the challenges of monitoring, as addressed here, what becomes clear is a need for more widespread monitoring of landslides and mega-gullies and documentation regarding the role of WRIFs. It is possible that a substantial fraction of the most hazardous mass movement events in cities are linked to WRIFs, and that significant hazard reduction can be realized by addressing WRIFs.

5 Conclusions

Urban development in Tijuana, Mexico was monitored for a five-year period to document the occurrence of mega-gullies and landslides, including sediment volumes. Over a five-year period with 14 storm events, two mega-gullies and one landslide were observed – and each occurring during a rainfall event. While the link between rainfall and erosion hazards is well known, monitoring showed that all three events were associated with a Water Resources Infrastructure Failure (WRIF). Mega-gullies occurred after a break in a water supply pipe, which unleashed a highly erosive, high-velocity water jet. Moreover, pipe breaks were observed to occur after rainfall and runoff formed a gully that undermined structural support for the water supply pipe. Hence, mega-gullies formed from a two-step process: (1) a water supply pipe breaks after the formation of a gully, and (2) a mega-gully is formed from the high velocity jet out of the water supply pipe. The observed landslide was also linked to a two-step process: (1) a water main leak saturated the hillslope creating the preconditions for a landslide, and (2) heavy rainfall triggered the landslide. Erosional features caused by WRIFs were larger than features generated by local rainfall and runoff, produced a significant amount of sediment on an event basis, and presented major safety hazards to downstream communities and ecosystems at the neighborhood and watershed scale. The limited data suggest that WRIF-based erosion events occur with an annual frequency of 40-60%, which is far higher than typical design standards for stormwater infrastructure (5-10% annual exceedance probability). Modeling shows that WRIFs contribute, on average, 5% of the total annual sediment generation at the watershed scale, and up to 58% on a storm-event basis. Additional research is needed to improve estimates of the spatial and temporal frequency of erosional features caused by WRIFs, and to understand the significance of WRIF hazards at other spatial and temporal scales and in other geographic contexts. Furthermore, the hazards posed by WRIFs within development on steep terrain calls for greater attention to infrastructure design and maintenance.

https://doi.org/10.5194/nhess-2021-47
Preprint. Discussion started: 15 March 2021

Structure from Motion (SfM) photogrammetric techniques helped to rapidly and safety assess the volume and shape of mega-gullies and landslides. Using imagery collected by either Unmanned Aerial Systems (UASs) or a camera on a hand-held pole, SfM techniques registered Digital Elevation Models (DEMs) with errors of ~3 cm horizontal RMSE and ~5 cm vertical RMSE which are in line with the needs for sediment budget applications.

Authors contribution

NG undertook data acquisition, processing and interpretation of the data, and prepared the manuscript with contributions from all co-authors. BS, TB and AG designed the research, and RB provided valuable guidance on the soil erosion modelling.

Competing interest

The authors declare that they have no conflicts of interest.

Acknowledgements

This study was funded by National Oceanic and Atmospheric Administration Ecological Effects of Sea Level Rise Program (award NA16NOS4780206), and the US Environmental Protection Agency (EPA) (Interagency Agreement ID # DW-12-92390601-0). The statements, findings, conclusions, and recommendations are those of the author(s) and do not necessarily reflect the views of NOAA or USEPA. We thank Kristine Taniguchi-Quan, Alejandro Hinojosa, Sergio Arregui, and Belinda Sandoval whose support on field collection and data analysis is gratefully acknowledged. We also thank Tijuana Metropolitan Planning Institute (IMPLAN) for data sharing. Special thanks to residents of Los Laureles Canyon, who provided valuable help for data collection.

References

Alfonso-Torreño, A., Gómez-Gutiérrez, A., Schnabel, S., Lavado-Contador, J. F., de San jose-Blasco, J. J., and Sánchez-Fernandez, M.: sUAS, SfM-MVS photogrammetry and a topographic algorithm method to quantify the volume of sediments retained in check-dams, Sci. Total Environ., 678, 369-382, https://doi.org/10.1016/j.scitotenv.2019.04.332, 2019.

Anderson, M. G., Holcombe, E., Holm-Nielsen, N., and Della Monica, R.: What Are the Emerging Challenges for Community-Based Landslide Risk Reduction in Developing Countries?, Nat. Hazards Rev., 15(2), 128–139, https://doi.org/10.1061/(ASCE)NH.1527-6996.0000125, 2014.

Ashmore, P.: Towards a sociogeomorphology of rivers, Geomorphology, 251, 149–156, https://doi.org/10.1016/j.geomorph.2015.02.020, 2015.

Biggs, T. W., Atkinson, E., Powell, R., and Ojeda-Revah, L.: Land cover following rapid urbanization on the US–Mexico border: Implications for conceptual models of urban watershed processes, Landsc. Urban Plan., 96(2), 78–87, https://doi.org/10.1016/j.landurbplan.2010.02.005, 2010.

Biggs, T. W., Anderson, W. G., and Pombo, O. A.: Concrete and Poverty, Vegetation and Wealth? A Counterexample from Remote Sensing of Socioeconomic Indicators on the U.S.–Mexico Border, The Professional Geographer, 1–14, https://doi.org/10.1080/00330124.2014.905161, 2014.

Biggs,T. W., Taniguchi, K. T., Gudino-Elizondo, N., Langendoen, E. J., Yuan, Y., Bingner, R. L., and Liden, D.: Runoff and Sediment Yield on the US-Mexico Border, Los Laureles Canyon, US Environmental Protection Agency, Report: EPA/600/R-18/365, Washington, DC, USA, 2018. Available online: https://cfpub.epa.gov/si/si_public_record_report.cfm?dirEntryId=343214&Lab=NERL, last access: October 3, 2020, 2017.

Bingner, R. L., Theurer, F. D., Yuan, Y., and Taguas, E.: AnnAGNPS Technical Processes, Washington, D.C. US Department of Agriculture (USDA)—Agricultural Research Service (ARS), Available online: https://www.wcc.nrcs.usda.gov/ftpref/wntsc/H&H/AGNPS/downloads/AnnAGNPS_Technical_Documentation.pdf, last access: 5 July 2020, 2015.

Borelli, S., Conigliaro, M., Quaglia, S., and Salbitano, F.: Urban and Peri-urban agroforestry as multifunctional land use. Agroforestry: Anecdotal to Modern Science, Springer Nature, Singapore, 705-725, https://doi.org/10.1007/978-981-10-7650-3_28, 2018.

Brand, M. W., Gudiño-Elizondo, N., Allaire, M., Wright, S., Matson, W., Saksa, P., and Sanders, B. F.: Stochastic Hydro-Financial Watershed Modeling for Environmental Impact Bonds, Water Resour. Res., 56, https://doi.org/10.1029/2020WR027328, 2020.

Calvello, M., Papa, M. N., and Pratschke, J.: Landslide risk perception: a case study in Southern Italy, Landslides, 13(2), 349–360, DOI 10.1007/s10346-015-0572-7, 2016.

Carrera-Hernández, J. J., Levresse, G., and Lacan, P.: Is UAV-SfM Surveying Ready to Replace Traditional Surveying Techniques?, Int. J. Remote Sens., 41 (12), 4818–4835, DOI:10.1080/01431161.2020.1727049, 2020.

Castillo, C., James, M. R., Redel-Macías, M. D., Pérez, R., and Gómez, J. A.: SF3M software: 3-D photo-reconstruction for non-expert users and its application to a gully network, The Soil, 1, 583–594, https://doi.org/10.5194/soil-1-583-2015, 2015.

Castillo, C., and Gómez, A.: A century of gully erosion research: Urgency, complexity and study approaches, Earth-Science Reviews, 160, 300–319, https://doi.org/10.1016/j.earscirev.2016.07.009, 2016.

Cook, P.: Infrastructure, rural electrification and development. Energy Sustain. Dev., 15, 304–313. http://dx.doi.org/10.1016/j.esd.2011.07.008, 2011.

Davis, M. L. (Eds): Planet of Slums, Verso, New York, USA, 2006.

Dietrich, J. T.: Riverscape mapping with helicopter-based Structure from-Motion photogrammetry, Geomorphology, 252, 144–157, https://doi.org/10.1016/j.geomorph.2015.05.008, 2016.

https://doi.org/10.5194/nhess-2021-47
Preprint. Discussion started: 15 March 2021

Eltner, A., Kaiser, A., Castillo, C., Rock, G., Neugirg, F., and Abellán, A.: Image-based surface reconstruction in geomorphometry – merits, limits and developments. Earth Surf. Dynam., 4: 359–389. https://doi.org/10.5194/esurf-4-359-2016, 2016.

Fu, S., Chen, L., Woldai, T., Yin, K., Gui, L., Li, D., Du, J., Zhou, C., Xu, Y., and Lian, Z.: Landslide hazard probability and risk assessment at the community level: A case of western Hubei, China, Nat. Hazards Earth Syst. Sci., 20, 581–601, https://doi.org/10.5194/nhess-20-581-2020, 2020.

Fugazza, D., Scaioni, M., Corti, M., D'Agata, C., Azzoni, R. S., Cernuschi, M., Smiraglia, C., and Diolaiuti, G.: A. Combination of UAV and terrestrial photogrammetry to assess rapid glacier evolution and map glacier hazards, Nat. Hazards Earth Syst. Sci., 18, 1055–1071, https://doi.org/10.5194/nhess-18-1055-2018, 2018.

Garrick, D. (2020). San Diego paying $2.5M fine for 2016 sewage spill in Tecolote Canyon, Mission Bay. The San Diego Union-Tribune, https://www.sandiegouniontribune.com/, last access 16 October 2020.

Gastil, R. G., Phillips, R. Allison, E.: Reconnaissance geology of the State of Baja California, Geological Society of America Memoir 140, 170, https://doi.org/10.1130/MEM140-p1, 1975.

Goodrich, K. A., Basolo, V., Feldman, D. L., Matthew, R. A., Schubert, J. E., Luke, A., Eguiarte, A., Boudreau, D., Serrano, K., Reyes, A. S. Contreras, S., Houston, D., Cheung, W., AghaKouchak A., and Sanders, B. F.: Addressing Pluvial Flash Flooding through Community-Based Collaborative Research in Tijuana, Mexico, Water, 12(5), 1257, https://doi.org/10.3390/w12051257, 2020.

Griffin, E., and Ford, L.: A model of Latin American city structure, Geogr. Rev., 70(4), 397–422, 1980.

Gudino-Elizondo, N., Biggs, T. W., Castillo, C., Bingner, R., Langendoen, E., Taniguchi, K., Kretzschmar, T., Yuan, Y., and Liden, D.: Measuring ephemeral gully erosion rates and topographical thresholds in an urban watershed using Unmanned Aerial Systems and structure from motion photogrammetric techniques, Land Degrad. Dev., 29, 1896 –1905, https://doi.org/10.1002/ldr.2976, 2018a.

Gudino-Elizondo, N., Biggs, T. W., Bingner, R. L., Yuan, Y., Langendoen, E. J., Taniguchi, K. T., Kretzschmar, T., Taguas, E. V., and Liden, D.: Modelling Ephemeral Gully Erosion from Unpaved Urban Roads: Equifinality and Implications for Scenario Analysis, Geosciences, 8, 137, https://doi.org/10.3390/geosciences8040137, 2018b.

Gudino-Elizondo, N., Kretzschmar, T., and Gray, S. C.: Stream flow composition and sediment yield comparison between partially urbanized and undisturbed coastal watersheds; case study: St. John, US Virgin Islands, Environ. Monit. Assess., 191:676, https://doi.org/10.1007/s10661-019-7778-4, 2019a.

Gudino-Elizondo, N., Biggs, T. W., Bingner, R. L., Yuan, Y., Langendoen, E. J., Kretzschmar, T., Taguas, E. V., Taniguchi, K. T., and Liden, D.: Modelling Runoff and Sediment Loads in a Developing Coastal Watershed of the US-Mexico Border, Water, 11, 1024, https://doi.org/10.3390/w11051024, 2019b.

Guo, S., Shao, Y., Zhang, T. Q., Zhu, D. Z., and Zhang, Y. P.: Physical modeling on sand erosion around defective sewer pipes under the influence of groundwater, J. Hydraul. Eng., 139(12), 1247–57, https://doi.org/10.1061/(ASCE)Hy.1943-7900.0000785, 2013.

Han, B., Wang, Z., Zhao, H., Jing, H., and Wu, Z.: Strain-Based Design for Buried Pipelines Subjected to Landslides, Pet. Sci., 9 (2), 236–241, DOI:10.1007/s12182-012-0204-y, 2012

Hardoy, J. E., Mitlin, D., Sattterwaite, D. (2nd Edition): Environmental Problems in an Urbanizing World, Routledge, London, UK, https://doi.org/10.4324/9781315071732, 2013.

Honegger, D. G., Hart, J. D., Phillips, R., Popelar, C., and Gailing, R. W.: Recent PRCI Guidelines for Pipelines Exposed to Landslide and Ground Subsidence Hazards: Proceedings of the 8th International Pipeline Conference, Calgary, AB, IPC2010-31311, 1-10, 2010.

Imwangana, F. M., Dewitte, O., Ntombi, M., and Moeyersons, J.: Topographic and road control of mega-gullies in Kinshasa (DR Congo). Geomorphology, 217, 131–139, https://doi.org/10.1016/j.geomorph.2014.04.021, 2014.

Ionita, I., Fullen, M. A., Zgłobicki, W., and Poesen, J.: Gully erosion as a natural and human-induced hazard, Nat. Hazards 79, DOI: 10.1007/s11069-015-1935-z, 2015.

Izumida, A., Uchiyama, S., and Sugai, T.: Application of UAV-SfM photogrammetry and aerial lidar to a disastrous flood: repeated topographic measurement of a newly formed crevasse splay of the Kinu River, central Japan, Nat. Hazards Earth Syst. Sci., 17, 1505–1519, https://doi.org/10.5194/nhess-17-1505-2017, 2017.

James, M. R., and Robson, S.: Straightforward reconstruction of 3D surfaces and topography with a camera: Accuracy and geosciences applications, J. Geophys. Res., 117, 1–17, https://doi.org/10.1029/2011JF002289, 2012.

James, M. R., and Robson, S.: Mitigating systematic error in topographic models derived from UAV and ground-based image networks, Earth Surf. Process. Landf., 39, 1413–1420, https://doi.org/10.1002/esp.3609, 2014.

James, M. R., Robson, S., d'Oleire-Oltmanns, S., and Niethammer, U.: Optimising UAV topographic surveys processed with structure-frommotion: Ground control quality, quantity and bundle adjustment, Geomorphology, 280, 51–66, https://doi.org/10.1016/j.geomorph.2016.11.021, 2017.

James, M. R., Chandler, J. H., Eltner, A., Fraser, C., Miller, P. E., Mills, J. P., Noble, T., Robson, S., and Lane, S. N.: Guidelines on the use of structure-from-motion photogrammetry in geomorphic research, Earth Surf. Process. Landf., 44 (10), 2081-2084, https://doi.org/10.1002/esp.4637, 2019.

Kaiser, A., Erhardt, A., Eltner, A.: Addressing uncertainties in interpreting soil surface changes by multitemporal high-resolution topography data across scales. Land Degrad. Dev., 29 (8), 2264-2277, https://doi.org/10.1002/ldr.2967, 2018.

Kim, K., Kim, J., Kwak, T. Y., and Chung, C. K.: Logistic regression model for sinkhole susceptibility due to damaged sewer pipes, Nat. Hazards, 93: 765–785, https://doi.org/10.1007/s11069-018-3323-y, 2018.

Kuo, H. L., Lin, G. W., Chen, C. W., Saito, H., Lin, C. W., Chen, H., and Chao, W. A.: Evaluating critical rainfall conditions for large-scale landslides by detecting event times from seismic records, Nat. Hazards Earth Syst. Sci., 18, 2877–2891, https://doi.org/10.5194/nhess-18- 2877-2018, 2018.

Luke, A., Sanders, B. F., Goodrich, K. A., Feldman, D. L., Boudreau, D., Eguiarte, A., Serrano, K., Reyes, A., Schubert, J. E., AghaKouchak, A., Basolo, V., and Matthew, R. A.: Going beyond the flood insurance rate map: insights from flood hazard map co-production, Nat. Hazards Earth Syst. Sci., 18(4), 1097-1120, https://doi.org/10.5194/nhess-18-1097-2018, 2018.

Ma, S., Wei, J., Xu, C., Shao, X., Xu, S., Chai, S., and Cui, Y.: UAV survey and numerical modeling of loess landslides: an example from Zaoling, southern Shanxi Province, China, Nat. Hazards, https://doi.org/10.1007/s11069-020-04207-1, 2020.

Marino, P., Peres, D. J., Cancelliere, A., Greco, R., and Bogaard, T. A.: Soil moisture information can improve shallow landslide forecasting using the hydrometeorological threshold approach, Landslides, DOI: 10.1007/s10346-020-01420-8, 2020.

Mazzoleni, M., Paron, P., Reali, A., Juizo, D., Manane, J., and Brandimarte, L.: Testing UAV-derived topography for hydraulic modelling in a tropical environment, Nat. Hazards, 103, 139–163, https://doi.org/10.1007/s11069-020-03963-4, 2020.

Miller, J. R., Ferri, K., Grow, D., and Villarroel, L.: Hydrologic, geomorphic, and stratigraphic controls on suspended sediment transport dynamics, Big Harris Creek restoration site, North Carolina, USA, Anthropocene, 25, https://doi.org/10.1016/j.ancene.2018.12.002, 2019.

McAdoo, B. G., Quak, M., Gnyawali, K. R., Adhikari, B. R., Devkota, S., Rajbhandari, P. L., and Sudmeier-Rieux, K.: Roads and landslides in Nepal: how development affects environmental risk, Nat. Hazards Earth Syst. Sci., 18, 3203–3210, https://doi.org/10.5194/nhess-18-3203-2018, 2018.

Minch, A. J., Ashby, J., Deméré, T., and Kuper, T.: Correlation and depositional environments of the Middle Miocene Rosarito Beach Formation of northwestern Baja California, Mexico, In: J.A. Minch and J.R. Ashby, Editors, Miocene and Cretaceous depositional environments, northwestern Baja California, Mexico: Pacific Section, American Association of Petroleum Geologists, 54, 33-46, 1984.

Nadal-Romero, E., Revuelto, J., Errea, P., and López-Moreno, J. I.: The application of terrestrial laser scanner and SfM photogrammetry in measuring erosion and deposition processes in two opposite slopes in a humid badlands area (central Spanish Pyrenees), The Soil, 1, 561–573, https://doi.org/10.5194/soil-1-561-2015, 2015.

Oliva-González, A. O., Jiménez, D. M., Alvarez-Garcia, I. N., Nicieza, C. G., and Álvarez-Vigil, A. E.: Hillside instability in the Tijuana metropolitan area. Analysis of landslide-provoked building collapse, Eng. Fail. Anal., 46, 166–178, https://doi.org/https://doi.org/10.1016/j.engfailanal.2014.08.004, 2014.

Peng, L., Lin, L., Liu, S. Q., and Xu, D.: Interaction between risk perception and sense of place in disaster-prone mountain areas: A case study in China's Three Gorges Reservoir Area, Nat. Hazards, 85(2), 777–792, DOI 10.1007/s11069-016-2604-6, 2017.

Poesen, J.: Soil erosion in the Anthropocene: Research needs, Earth Surf. Process. Landf., 43(1), 64–84, https://doi.org/10.1002/esp.4250, 2018.

Retief, F., Bond, A., Pope, J., Morrison-Saunders, A., and King, N.: Global megatrends and their implications for environmental assessment practice, Environ. Impact Assess. Rev., 61:52–60, https://doi.org/10.1016/j.eiar.2016.07.002, 2016.

Sepúlveda, S. A., and Petley, D. N.: Regional trends and controlling factors of fatal landslides in Latin America and the Caribbean, Nat. Hazards Earth Syst. Sci., 15(8), 1821–1833, https://doi.org/10.5194/nhess-15-1821-2015, 2015.

Sidle R, Furuichi T, and Kono Y.: Unprecedented rates of landslide and surface erosion along a newly constructed road in Yunnan, China. Nat. Hazards, 57, 313–326, DOI: 10.1007/s11069-010-9614-6, 2011.

https://doi.org/10.5194/nhess-2021-47
Preprint. Discussion started: 15 March 2021

Taniguchi, K. T., Biggs, T. W., Langendoen, E. J., Castillo, C., Gudino-Elizondo, N., Yuan, Y., and Liden, D.: Stream channel erosion in a rapidly urbanizing region of the US–Mexico border: Documenting the importance of channel hardpoints with Structure from-Motion photogrammetry, Earth Surf. Process. Landf, 43, 1465–1477, https://doi.org/10.1002/esp.4331, 2018.

USDA (2018). Estimating Moist Bulk Density by Texture. https://www.nrcs.usda.gov/wps/portal/nrcs/detail/soils/survey/office/ssr10/tr/?cid=nrcs144p2_074844, last access: 3 September 2019.

USGS (2021). Landslide Hazard Information. https://geology.com/usgs/landslides/, last access: 22 January 2021.

Valentin, C., Poesen, J., and Li, Y.: Gully erosion: Impacts, factors and control, Catena 63, 132–153, https://doi.org/10.1016/j.catena.2005.06.001, 2005.

Valenzuela, P., Domínguez-Cuesta, M. J., García, M. A. M., and Jiménez-Sánchez, M.: Rainfall thresholds for the triggering of landslides considering previous soil moisture conditions (Asturias, NW Spain), Landslides, 15 (2), 273–282, DOI 10.1007/s10346-017-0878-8., 2018.

Van Zyl, J. E., Alsaydalani, M. O., Clayton, C. R., Bird, T., and Dennis, A.: Soil fluidisation outside leaks in water distribution pipes—Preliminary observations, J. Water Manage., 166(10), 546–555, https://doi.org/10.1680/wama.11.00119, 2013.

Vigiak, O., Borselli, L., Newham, L. T. H., McInnes, J., and Roberts, A. M.: Comparison of conceptual landscape metrics to define hillslope-scale sediment delivery ratio, Geomorphology, 138, 74–88, https://doi.org/10.1016/j.geomorph.2011.08.026, 2012.

Weis, D. A., Callaway, J. C., and Gersberg, R. M.: Vertical accretion rates and heavy metal chronologies in wetland sediments of the Tijuana Estuary, Estuaries, 24, 840–850, https://doi.org/10.2307/1353175, 2001.

Wheaton, J. M., Brasington, J., Darby, S. E., and Sear, D. A.: Accounting for uncertainty in DEMs from repeat topographic surveys: improved sediment budgets, Earth Surf. Process. Landf., 35, 136–156, https://doi.org/10.1002/esp.1886, 2010.

Whittington, D., Davis, J., Prokopy, L., Komives, K., Thorsten, R., Lukacs, H., Bakalian, A., and Wakeman, W.: How well is the demand-driven, community management model for rural water supply systems doing? Evidence from Bolivia, Peru and Ghana, Water Policy, 11(6): 696-718. DOI: 10.2166/wp.2009.310, 2009.

Xu, X., Zhang, H., Wang, W. Zhao, C., and Yan, Q.: Quantitative monitoring of gravity erosion using a novel 3D surface measuring technique: validation and case study, Nat. Hazards, 75(2), 1927–1939, DOI: 10.1007/s11069-014-1405-z, 2015.

Zhuo, L., Dai, Q., Han, D., Chen, N., Zhao, B., and Berti, M.: Evaluation of remotely sensed soil moisture for landslide hazard assessment. IEEE J. Sel. Top. Appl. Earth Obs. Remote Sens., https://doi.org/10.1109/JSTARS.2018.2883361, 2019.